Thickness, stability and contact angle of liquid films on and inside nanofibres, nanotubes and nanochannels

Davide Mattia,[a*] *Victor Starov*,[b] *Sergey Semenov*[b]

[a]Department of Chemical Engineering, University of Bath, BA27AY, UK, d.mattia@bath.ac.uk

[b]Department of Chemical Engineering, Loughborough University, LE113TU, UK,

V.M.Starov@lboro.ac.uk

[*] Corresponding author: Davide Mattia, ph.: +44(0)1225-383961; fax: +44(0)1225-385713

Abstract

While the stability of liquid films on substrates is a classical topic of colloidal science, the availability of nanostructured materials, such as nanotubes, nanofibers and nanochannels, has raised the question of how the stability of liquid films and their wetting behaviour is affected by nanoscale confinement. This paper will present the conditions for the stability of liquid films on and inside cylindrical solid substrates with nanometre scale characteristic dimensions. It is shown that the stability is determined by an effective disjoining/conjoining pressure isotherm which differs from the corresponding disjoining/conjoining pressure isotherm of flat liquid films on *flat* solid substrates. From the former, the equilibrium contact angles of drops on an outer or inner surface of a cylindrical capillary have been calculated as a function of surface curvature, showing that the expressions for equilibrium contact angles vary for different geometries, in view of the difference in thickness of the film of uniform thickness with which the bulk liquid (drops or menisci) is at equilibrium. These calculations have been extended to the case of glass nanocapillaries and carbon nanotubes, finding good agreement with experimental results in the literature.

Keywords: disjoining pressure; wetting; capillary filling; carbon nanotubes; carbon nanofibers

1. Introduction

The stability of liquid films on substrates is a classic topic of colloidal science and a vast literature exists on the subject (see [1, 2] and the references wherein). An area of renewed interest is understanding how the stability of liquid films and their wetting behaviour is affected by nanoscale confinement of liquids on or inside nanofibers, nanotubes or nanochannels [3, 4].

How fluids wet nanofibers, for example, is of primary importance in the area of composite materials, where a strong adhesion between the matrix and the fibre is essential for effective load transfer [5-7]. In the case of carbon nanotube (CNT) – polymer matrix composites, the key to a successful load transfer between the matrix and the fibre reinforcement has been the ability of the matrix material to wet the CNTs [8, 9]. To achieve this result, chemical modification of polymer matrixes has often been required to change their wetting behaviour. An example of the latter is the observation via environmental scanning electron microscopy (ESEM) of the difference in the contact angle of pure and modified PVDF nanodroplets on CNTs [7]. Similar results have been obtained with different combinations of nanotubes, nanofibers and polymer matrixes [10]. Conversely, polymers have been used to alter the wettability of nanotubes, in particular concerning their dispersability in aqueous media. An example is the addition of anti-foaming agents to improve the dispersability of CNTs in dispersions via ultra-sonication by eliminating air trapped at the CNTs surface [11].

Nanoscale confinement appears to have a significant effect on the filling of nanotubes and nanopores [3, 4, 12]. Molecular dynamics simulations have shown the presence of a monolayer of liquid adsorbed on the wall in the capillary filling of nanochannels, leading to the deformation of the meniscus profile from the ideal circular cross-section [13]. This distortion has been attributed to the disjoining pressure induced by molecular interactions between the fluid and the channel wall [1, 2]. Some evidence of the formation of precursor layers in the capillary filling of nanochannels has been obtained via ESEM studies of preferential condensation of water inside hydrophilized CNTs [14, 15]. Density functional theory calculations have also shown that these layers would have reduced viscosity compared to the 'bulk' fluid and that their stability would endure beyond the initial capillary filling stage [16, 17]. As the thickness of these precursor layers or any other thin liquid film approaches the nanometre scale, the effect of long-range forces (van der Waals, electrical double layer and structural forces) becomes significant. Their effect on macroscopic wetting is well known and can be described using the disjoining/conjoining pressure [18]. Recently, the effect on wetting of nanometre scale films of the presence of nanoparticle dispersions has been investigated, showing that for film thicknesses comparable with the nanoparticle size, the latter tends to assume an ordered structure, reducing film pressure and, thereby, increasing the spreading of the liquid [19].

The validity of the above results is limited to the continuum model regime. For nanoscale

confinement inside CNTs, the size threshold below which the continuum model no longer can be applied has been calculated, using molecular dynamics, as about 2nm[3, 4, 20]. Some experimental evidence of this limit has been observed in transmission electron microscope (TEM) micrographs of water plugs inside ~2 nm diameter carbon nanotubes, where a continuous, well defined liquid meniscus could not be observed [21, 22].

In all these areas the stability of liquid films represents a key factor in understanding the effect of nanoscale confinement on liquid wetting. This paper presents the conditions for the stability of liquid films on and inside cylindrical solid substrates, with particular emphasis on nanometre scale substrates. It is shown that the stability is determined by an effective disjoining/conjoining pressure isotherm, $\Pi_{eff}(h)$, which differs from the corresponding disjoining/conjoining pressure isotherm of flat liquid films on *flat* solid substrates.

2. Liquid profiles on a curved surface: derivation of governing equations.

The excess free energy of a liquid droplet on the outer surface of a cylindrical capillary of radius a is as follows

$$\Phi = 2\pi\gamma\int_0^\infty\left[(a+h)\sqrt{1+h'^2}-(a+h_e)\right]dx+$$
$$+\pi P_e\int_0^\infty\left[(a+h)^2-(a+h_e)^2\right]dx+ \qquad (1)$$
$$+2\pi a\int_0^\infty\left[\int_h^\infty\Pi(h)\,dh-\int_{h_e}^\infty\Pi(h)\,dh\right]dx$$

where the outer surface of the cylindrical capillary covered by the equilibrium liquid film of the thickness h_e was selected as a reference state; x is in the direction parallel to the cylinder axis (Fig. 1).

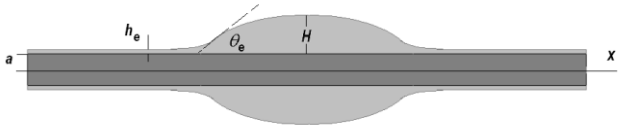

Fig. 1. Cross section of an axi-symmetric liquid droplet on the outer surface of a cylinder of radius *a*. H – the maximum height of the droplet, h_e – the thickness of an equilibrium film of a uniform thickness, h_e.

In Eq. (1), the first term represents the excess of the surface energy as compared with the surface energy of the flat equilibrium liquid film; the second term is the excess energy associated with the excess of the drop volume as compared with the volume of the flat film; the third term represents the excess of the energy caused by the surface forces action again as compared with the excess in the flat films.

The conditions of equilibrium are as follows [2]:

(A) $\delta\Phi = 0$ or $\frac{\partial f}{\partial h} - \frac{d}{dx}\frac{\partial f}{\partial h'} = 0$

(B) $\frac{\partial^2 f}{\partial h'^2} > 0$,

where,

$$f = 2\pi\gamma\left[(a+h)\sqrt{1+h'^2} - (a+h_e)\right] + \pi P_e\left[(a+h)^2 - (a+h_e)\right] + 2\pi a\left[\int_h^\infty \Pi(h)\,dh - \int_{h_e}^\infty \Pi(h)\,dh\right]$$

(C) The solution of the Jacoby's equation, *u(x),* should not vanish at any position *x* inside the region under consideration, except for boundaries of the region of integration in Eq. (1),

(D) The transversality condition at the apparent three phase contact line should be satisfied. The transversality condition provides the condition of a smooth transition from a non-flat liquid profile to a flat equilibrium film in front [2]. The transversality condition reads $\left[f - h'\frac{\partial f}{\partial h'} \right]_{x=\Re} = 0$, where $\Re$ is the position of the three phase contact line.

Condition (A) results in the following equation describing the liquid profile on the surface of the cylindrical capillary:

$$\frac{\gamma h''}{\left(1+h'^2\right)^{3/2}} - \frac{\gamma}{(a+h)\sqrt{1+h'^2}} + \frac{a}{a+h}\Pi(h) = P_e \qquad (2)$$

Note that the latter equation is different from the corresponding equation for the case of flat surfaces [2],

$$\frac{\gamma h''}{\left(1+h'^2\right)^{3/2}} + \Pi(h) = P_e \qquad (3)$$

not only because of the presence of the second curvature, $-\frac{\gamma}{(a+h)\sqrt{1+h'^2}}$, but also because of a difference in the definition of the disjoining pressure, which is now $\frac{a}{a+h}\Pi(h)$ instead of $\Pi(h)$ in Eq. (3). The latter difference results in substantial consequences as shown below in the case of thin

capillaries. It is also pointed out that the excess pressure, P_e, is determined by the vapour pressure in the surrounding air and is given by Kelvin's equation [2]:

$$P_e = \frac{RT}{v_m} \ln \frac{p_s}{p} \tag{4}$$

where *R, T,* and v_m are the universal gas constant, the absolute temperature, and the liquid molar volume, respectively; p_s and p are the pressures of the saturated vapour and the vapour with which the liquid film is in equilibrium, respectively. The latter expression shows that the excess pressure, P_e, cannot be fixed arbitrary, but is determined by the vapour pressure in the ambient air, p. Note also that the Kelvin's equation expresses the equality of chemical potentials of liquid molecules in vapour and liquid phases. Hence, in the case of droplets on a cylindrical capillary, as in the case of droplets on flat solid substrates, the equilibrium is possible only at over-saturation, that is, at $P_e < 0$.

2.1 Effective disjoining/conjoining pressure – outer surface of a cylindrical capillary

Consider the equilibrium film of uniform thickness h_e on the outer surface of a cylindrical capillary shown in Fig. 1. It follows from Eq. (2) that

$$-\frac{\gamma}{\left(a+h_e\right)} + \frac{a}{a+h_e}\Pi(h_e) = P_e \tag{5}$$

Let us introduce an effective disjoining/conjoining pressure as:

$$\Pi_{eff}(h) = -\frac{\gamma}{\left(a+h\right)} + \frac{a}{a+h}\Pi(h) \tag{6}$$

We show below that the above introduced effective disjoining pressure provides the correct stability conditions for a film of a uniform thickness on a cylindrical surface. For that purpose consider the excess free energy per unit length of the capillary of the equilibrium film of a uniform thickness, h_e:

$$\Phi_e = 2\pi\gamma(a+h_e) + \pi P_e\left[\left(a+h_e\right)^2 - a^2\right] + 2\pi a\int_{h_e}^{\infty}\Pi(h)dh + 2\pi a\left(\gamma_{sl}-\gamma_{sv}\right) \tag{7}$$

where γ_{sl} and γ_{sv} are the solid-liquid and solid-vapour interfacial tensions, respectively. According to the equilibrium requirements the following conditions should be satisfied [2]:

$$\frac{d\Phi_e}{dh_e} = 0 \text{ and } \frac{d^2\Phi_e}{dh_e^2} > 0 \tag{8}$$

The first condition results in:

$$\gamma + P_e(a+h_e) - a\Pi(h_e) = 0 \Leftrightarrow \Pi_{eff}(h_e) = P_e \tag{9}$$

where the definition of the effective disjoining pressure in Eq. (6) has been used. The second equilibrium condition yields

$$P_e - a\Pi'(h_e) > 0 \tag{10}$$

The effective disjoining/conjoining pressure isotherm defined in Eq. (6) satisfies the stability condition Eq. (8). In fact:

$$\frac{d\Pi_{eff}}{dh_e} = -\frac{a}{(a+h_e)^2}\left[\Pi(h_e) - \frac{\gamma}{a}\right] + \frac{a}{a+h_e}\Pi'(h_e) \tag{11}$$

Substitution of the expression for $\Pi(h_e)$ from Eq. (5) yields

$$\frac{d\Pi_{eff}}{dh_e} = -\frac{a}{(a+h_e)^2}\left[\left(\frac{\gamma}{a} + P_e\frac{a+h_e}{a}\right) - \frac{\gamma}{a}\right] + \frac{a}{a+h_e}\Pi'(h_e) = \frac{1}{a+h_e}\left[a\Pi'(h_e) - P_e\right] < 0 \tag{12}$$

according to condition (10). Hence, we conclude that

$$\frac{d\Pi_{eff}}{dh_e} < 0 \tag{13}$$

The latter means that the introduced effective disjoining/conjoining pressure according to Eq. (6) possesses all necessary properties according to equilibrium conditions in Eq. (8). This effective disjoining/conjoining pressure isotherm will be used in Section 3 to investigate the stability of uniform liquid films on cylindrical surfaces.

2.2 Effective disjoining/conjoining pressure – inner surface of a cylindrical capillary

In the case of liquid layers inside the inner part of the capillary of radius *a*, the excess free energy is defined as:

$$\begin{aligned}\Phi = {} & 2\pi\gamma\int_0^\infty\left[(a-h)\sqrt{1+h'^2} - (a-h_e)\right]dx + \\ & +\pi P_e\int_0^\infty\left[(a-h_e)^2 - (a-h)^2\right]dx \\ & +2\pi a\int_0^\infty\left[\int_h^\infty\Pi(h)\,dh - \int_{h_e}^\infty\Pi(h)\,dh\right]dx\end{aligned} \tag{14}$$

which is similar to the expression for the excess free energy on the outer cylindrical surface Eq. (1) with terms defined in Fig. 2.

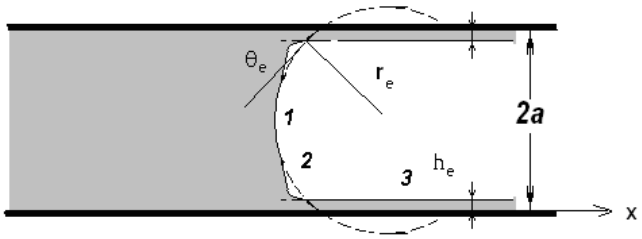

Fig. 2. Profile of a meniscus in a cylindrical capillary of radius a. 1 – a spherical part of the meniscus of curvature r_e; 2 – transition zone between the spherical meniscus and flat films in front; 3 – flat equilibrium liquid film of thickness h_e.

Following the same procedure for the case of the outer cylindrical surface the following equation for the liquid meniscus profile inside a capillary can be deduced:

$$\frac{\gamma h''}{\left(1+h'^2\right)^{3/2}} + \frac{\gamma}{(a-h)\sqrt{1+h'^2}} + \frac{a}{a-h}\Pi(h) = P_e \qquad (15)$$

The equation above is different from both equations for a liquid on the outer cylindrical surface and on a flat surface, Eq.s (2) and (3), respectively. The effective disjoining isotherm for this case is defined as

$$\Pi_{eff}(h) = \frac{a}{a-h}\Pi(h) + \frac{\gamma}{(a-h)} \qquad (16)$$

The corresponding expression for the excess free energy per unit length of a uniform film on the inner cylindrical surface is

$$\Phi_e = 2\pi\gamma(a-h_e) + \pi P_e\left[a^2 - (a-h_e)^2\right] + 2\pi a\int_{h_e}^{\infty}\Pi(h)\,dh + 2\pi a\left(\gamma_{sl}-\gamma_{sv}\right) \qquad (17)$$

The latter expression and the definition in Eq. (16) result in the usual conditions in Eq. (8) which describe the stability of the film of a uniform thickness on the inner surface of a cylindrical capillary.

3. Equilibrium contact angle of a droplet on the outer surface of a cylindrical capillary

The effective disjoining/conjoining pressure term in Eq. (6) can be used to calculate the equilibrium contact angle for the droplet profile in Fig. 1, described by Eq. (2). Let H be the maximum height of the droplet in the centre, that is $h(0) = H$. Let us introduce a new unknown function $u = \frac{1}{\sqrt{1+h'^2}}$ in this equation and integrate Eq. (2) once, which results in

$$\frac{1}{\sqrt{1+h'^2}} = 1 + \frac{P_e\left(\frac{H^2}{2} + aH - ah - \frac{h^2}{2}\right) - \int_h^\infty \Pi(h)\,dh}{\gamma(a+h)} \tag{18}$$

where the condition $h'(H) = 0$ is taken into account. If the disjoining/conjoining pressure in the right hand side of the equation is neglected, the 'outer solution' is obtained, which describes the drop profile not distorted by the disjoining/conjoining pressure action:

$$\frac{1}{\sqrt{1+h'^2}} = 1 + \frac{P_e\left(\frac{H^2}{2} + aH - ah - \frac{h^2}{2}\right)}{\gamma(a+h)} \tag{19}$$

Prolonging the above 'outer solution' to the intersection with the surface of the cylinder, one obtains $h'(0) = -\tan\theta_e$, where θ_e is the equilibrium contact angle to be determined. Using the latter condition in Eq. (19) one obtains:

$$\cos\theta_e = 1 + \frac{P_e\left(\frac{H^2}{2} + aH\right)}{\gamma a} \text{ or } P_e = \frac{(\cos\theta_e - 1)2\gamma a}{H^2 + 2aH} < 0 \tag{20}$$

Now from the whole Eq. (18) it can be concluded that the local profile tends asymptotically to the film of uniform thickness, h_e. That is, locally the profile satisfies the condition $h'(h_e) = 0$. Using this condition it can be concluded that:

$$0 = \frac{P_e\left(\frac{H^2}{2} + aH - ah_e - \frac{h_e^2}{2}\right) - a\int_{h_e}^\infty \Pi(h)\,dh}{\gamma(a+h_e)} \text{ or } P_e\left(\frac{H^2}{2} + aH - ah_e - \frac{h_e^2}{2}\right) - a\int_{h_e}^\infty \Pi(h)\,dh = 0 \tag{21}$$

where the equilibrium thickness of the uniform film is determined from the following equation:

$$\Pi_{eff}(h_e) = -\frac{\gamma}{(a+h_e)} + \frac{a}{a+h_e}\Pi(h_e) = P_e \tag{22}$$

Substitution of Eq. (21) into Eq. (20) results in the following equation for the determination of the equilibrium contact angle:

$$\cos\theta_e = 1 + \frac{1}{1 - \frac{2ah_e + h_e^2}{H^2 + 2aH}} \frac{1}{\gamma}\int_{h_e}^\infty \Pi(h)\,dh \tag{23}$$

If the term $\frac{2ah_e + h_e^2}{H^2 + 2aH} = \frac{h_e}{H}\frac{2a + h_e}{H + 2a} \sim \frac{h_e}{H}$ in the latter equation is small, one obtains

$$\cos\theta_e \approx 1 + \frac{1}{\gamma}\int_{h_e}^\infty \Pi(h)\,dh \tag{24}$$

The functional form of the latter equation is identical to the corresponding expressions for the contact angle of a meniscus in a flat capillary and a droplet on a flat substrate [2]. However, there is a substantial difference between the former and the latter cases: while the lower limit of integration

is the thickness of the uniform film for all mentioned cases, its value is substantially different in each equation. This value is determined by the disjoining/conjoining pressure isotherm for flat liquid films, and by the effective disjoining/conjoining pressure for curved geometries, as discussed above. In the particular case of a droplet on a cylindrical surface (Fig. 1) the thickness of the liquid film should be determined from Eq. (22).

Eq. (24) shows that, indeed, liquid droplets on the outer surface of a cylinder can be at the equilibrium only at over-saturation as droplets on a flat substrate. This condition has been observed experimentally for water droplets on large carbon nanotubes [15]. Furthermore, analysis of ESEM micrographs of frozen benzene droplets on CNTs supports this conclusion (Fig. 3a). A drop of hydrocarbon-CNT dispersion was placed on a Peltier cooling stage in the ESEM and the temperature rapidly brought to 2 °C, below the freezing temperature of both liquids. Increasing the temperature close to the freezing temperature actually led to the immediate evaporation of the hydrocarbons due to their low saturation in the ESEM chamber, rather than a slow transition from solid to liquid phase. The presence of a thin film enveloping the CNT as a smooth continuation of the drop can also be seen in Fig. 3b. Similar methods have also been used to investigate the wetting of polymers on fibres and nanotubes to assess the effectiveness of load transfer from the matrix to the fibre reinforcement [23, 24].

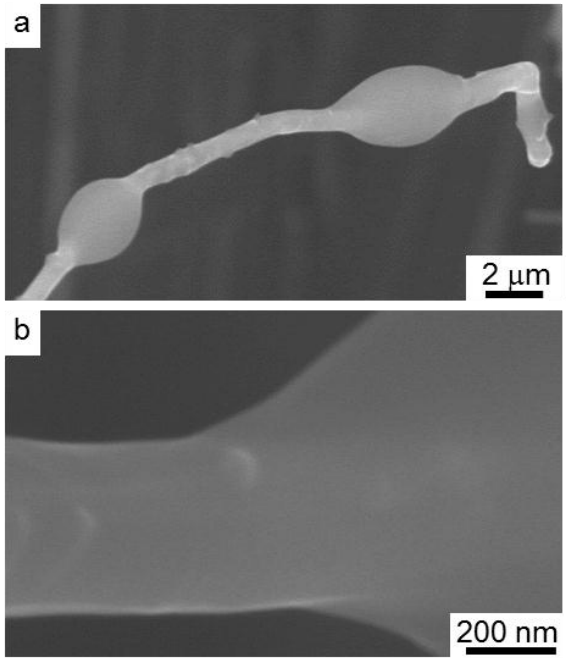

Fig. 3. a) ESEM micrograph of two frozen benzene drops around a CNT; b) detail of the intersection of a cyclohexane droplet with the outer region of a CNT.

4. Equilibrium contact angle of a liquid meniscus inside a cylindrical capillary

The meniscus profile of a liquid plug inside a cylindrical capillary is described by Eq. (15). As in the case of droplet on a cylindrical surface, an unknown function $u = \frac{1}{\sqrt{1+h'^2}}$ is introduced. After one integration, Eq. (15) takes the following form

$$\frac{1}{\sqrt{1+h'^2}} = \frac{\frac{P_e}{2}(a-h)^2 - a\int_h^\infty \Pi(h)dh}{\gamma(a-h)} \tag{25}$$

where the condition in the centre of the capillary $h'(a) = -\infty$ is already taken into account. Neglecting the disjoining pressure in the above equation yields

$$\frac{1}{\sqrt{1+h'^2}} = \frac{P_e(a-h)}{2\gamma} \tag{26}$$

which describes the profile of a spherical meniscus. Continuation of this profile to the intersection with the capillary surface results, as in the previous case, in

$$\cos\theta_e = \frac{P_e a}{2\gamma} \Leftrightarrow P_e = \frac{2\gamma\cos\theta_e}{a} > 0, \tag{27}$$

as expected. Note that the latter equation means that the equilibrium meniscus exists at undersaturation only. From the whole Eq. (25) one concludes that the local profile tends asymptotically to the film of uniform thickness, h_e. That is, locally the profile satisfies the condition $h'(h_e) = 0$. Using this condition and Eq. (27) it can be seen from Eq. (25) that

$$\cos\theta_e = \frac{1}{1-\frac{h_e}{a}} + \frac{1}{\left(1-\frac{h_e}{a}\right)^2}\frac{1}{\gamma}\int_{h_e}^\infty \Pi(h)dh \tag{28}$$

where the thickness of the uniform film is determined from

$$\Pi_{eff}(h_e) = \frac{a}{a-h_e}\Pi(h_e) + \frac{\gamma}{(a-h_e)} = P_e \tag{29}$$

Assuming that $h_e \ll a$ in Eq. (28) the same functional dependence of the $\cos\theta_e$ as in Eq. (24) is obtained. However, the equilibrium thickness of a flat film should now be determined from Eq. (29). Observing Eq.s (24) and (28), a significant difference exists between the equilibrium of drops and menisci: in the former case (both for a flat or outer cylindrical substrate) the external supersaturated vapour pressure in the ambient air may be arbitrary inside narrow limits, which can be exactly determined, as detailed elsewhere [2]. The drop size adjusts to the imposed oversaturated pressure at equilibrium. The situation is very much different in the case of an equilibrium meniscus inside a

capillary (both for a slit or circular capillary): there is only a unique vapour pressure allowing the meniscus to be at equilibrium. At all other vapour pressures, the meniscus cannot be at equilibrium. This phenomenon has indeed been observed experimentally by studying the condensation of water inside large carbon nanotubes (200 nm diameter) in the ESEM [14]: For a given temperature, a liquid film forms initially on the nanotube walls; the film then thickens with increasing partial pressure of water vapour in the ESEM chamber and then jumps to form a liquid plug occupying the entire bore of the tube. Upon reduction of the vapour partial pressure, the plug breaks up thinning down to a film of thickness approximately equal to the initial one [25]. Similar results have been observed also for smaller CNTs (40-60 nm diameter) [15].

5. Thermodynamic Stability of thin liquid films on the outer surface of a cylindrical capillary

The thermodynamic stability of thin liquid layers on the outer surface of a cylindrical capillary is considered below. Let a be the radius of the capillary. If the film thickness, h, is much smaller than the radius, $h \ll a$, as a first approximation the isotherm of the disjoining pressure of a planar layer, $\Pi(h)$, can be used. However, in the general case, the disjoining pressure in thin liquid films on a curved substrate, Π_a, is different from the corresponding disjoining pressure on a flat surface. An estimation of the distortion of dispersion forces on curved surfaces has been reported elsewhere [2]: It has been shown that at $h/a \le 0.2$, the difference between Π_a and Π does not exceed 2.5%. It is shown below that capillary effects, on the other hand, have considerably more pronounced influence on the thickness and stability of films on non-planar surfaces. Therefore, in the subsequent calculations, the disjoining/conjoining pressure isotherm of flat liquid films, $\Pi(h)$, is used.

Let us first examine equilibrium films on the convex surface of a cylinder with a radius a. The conditions of the equilibrium for a film on a convex surface of a cylinder of radius a have the form given by Eq.s (9) and (13) where the effective isotherm of disjoining/conjoining pressure is given by Eq. (6). The latter can be rewritten as:

$$\Pi_{eff}(h) = \frac{a}{a+h}\left[\Pi(h) - \frac{\gamma}{a}\right] \tag{30}$$

According to the previous equation, $\Pi_{eff}(h)$ vanishes at $\Pi(h) = \gamma / a$. If we adopt $\Pi(h) = \frac{A}{h^3}$ where A is the Hamaker constant, then

$$\Pi_{eff}(h) = \frac{a}{a+h}\left[\frac{A}{h^3} - \frac{\gamma}{a}\right] \text{ and } \Pi_{eff}(h) = 0 \Leftrightarrow h_0 = \left(\frac{aA}{\gamma}\right)^{1/3} \tag{31}$$

The effective disjoining/conjoining pressure isotherm according to Eq. (31) is shown in Fig. 4.

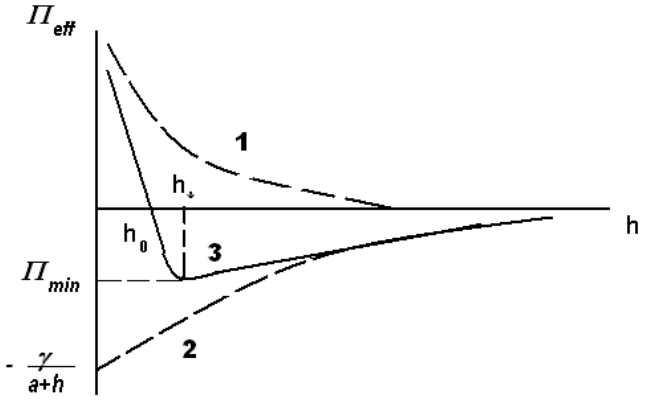

Fig. 4. Effective disjoining/conjoining pressure isotherm $\Pi_{eff}(h)$: Curve 3 according to Eq. (31). Curves 1 and 2 are for $\frac{A}{h^3}$ and $-\frac{\gamma}{a+h}$, respectively.

For the benzene/CNT system reported in Fig. 3, one can assume $a = 100$ nm, $\gamma = 29 \cdot 10^{-3}$ Nm^{-1} and $A \sim 10^{-20}$ J [26]. According to Eq. (31) then, $h_0 \sim 3.5$ nm, which is consistent with analysis of ESEM micrographs. This result can be generalized by stating that at the saturation, $p/p_s = 1$, the film on a curved surface does not tend to an infinity (as on a flat surface) but tends to a finite thickness h_0.

It is interesting to notice that in the case of complete wetting, $\Pi(h) = \frac{A}{h^3}$, the equilibrium adsorption does not take place under over-saturation on a flat surface. However, according to the effective disjoining/conjoining pressure given by Eq. (30) the adsorption is possible on an outer cylindrical surface at over-saturations in the range from $p/p_s = 1$ to $p/p_s = \exp\left(\frac{\Pi_{\min} v_m}{RT}\right) > 1$. The adsorption films, though, are stable only in the region of thicknesses where the stability condition Eq. (13) is satisfied. Using this condition, it can be shown that in the case $h \ll a$ the critical thickness for the isotherm corresponding to complete wetting according to Eq. (31) is (Fig. 4):

$$\Pi'_{eff}(h^*) = 0 \Rightarrow h^* \approx \left(\frac{3a^2 A}{\gamma}\right)^{1/4} \qquad (32)$$

The latter conclusion has been verified experimentally for decane films on cylindrical quartz capillaries [27]: For a capillary radius $a = 100$ nm, $\gamma = 23 \cdot 10^{-3}$ Nm^{-1} and $A = 1.6 \cdot 10^{-20}$ J, a critical film thickness $h^* \approx 12$ nm was obtained.

However, the loss of stability occurs only at $\Pi_{eff}(h) < 0 \Leftrightarrow p/p_s > 1$, i.e., in the region of oversaturation. When $p/p_s < 1$, the films remain stable, but their thickness (in contrast to planar films) does not tend to infinity as $p/p_s \to 1$, rather toward a limiting value $h_0 = \left(\frac{Aa}{\gamma}\right)^{1/3}$. In the

case of partial wetting the solution is far more difficult to obtain because the shape of the disjoining/conjoining isotherm is more complex [2].

6. Thermodynamic Stability of thin liquid films inside a cylindrical capillary

The effective disjoining pressure isotherm, $\Pi_{eff}(h)$, on the inner surface of a cylindrical capillary of radius a will now be considered. The equation for equilibrium of liquid and vapour in this case is, according to Eq. (16):

$$\frac{a}{a-h}\left(\Pi(h)+\frac{\gamma}{a}\right)=\Pi_{eff}(h)=P_e \tag{33}$$

The corresponding stability condition is given by Eq. (13). In contrast to convex surfaces (outer cylindrical surface), the film thickness h is evidently limited by the value of the capillary radius. However, long before h approaches the inner radius of the capillary it becomes necessary to account for the influence of overlapping fields of surface forces of all sections of the capillary surface. For slit pores, the corresponding evaluations have already been undertaken [28].

6.1 Complete Wetting Case

In the case of complete wetting the isotherm of disjoining pressure for the flat film is $\Pi(h)=\frac{A}{h^3}$.

According to condition (13) the critical thickness h^* can be calculated when the film of a uniform thickness on the inner surface loses its stability. Based on Eq. (16) one can conclude that:

$$\Pi'_{eff}(h^*)=0 \Leftrightarrow \frac{A}{h^{*3}}+\frac{\gamma}{a}=\frac{3A(a-h)}{h^{*4}} \tag{34}$$

If one can assume that $h \ll a$, then the critical thickness is:

$$h^*=\left(\frac{3a^2A}{\gamma}\right)^{1/4} \tag{35}$$

In Fig. 5 a schematic dependency of the effective disjoining/conjoining pressure isotherm is shown.

As an example, the thickness h of stable water films on the inner surface of a quartz capillary as a function of the relative vapour pressure p/p_s is shown in Figure 6. The curves are plotted on the basis of Eq. (16), using $\Pi(h)=\frac{A}{h^3}$, and P_e replaced by its values from Eq. (4) which results in

$$\frac{a}{a-h}\left(\frac{A}{h^3}+\frac{\gamma}{a}\right)=\frac{RT}{v_m}\ln\frac{p_s}{p} \tag{36}$$

using $v_m = 18\ \mathrm{cm}^3/\mathrm{mol}$, $T = 293\ \mathrm{K}$, $\gamma = 72 \cdot 10^{-3}\ \mathrm{Nm}^{-1}$ and $A = 7 \cdot 10^{-21}\ \mathrm{J}$ [29]. Curve 4 in Fig. 6 is the isotherm $h(p/p_s)$ for a planar surface, when $a = \infty$. Curves 1, *2* and *3* were plotted for capillaries with radius a equal to 1, 10 and 100 nm, respectively. Whereas the curve for the largest capillary radius (curve *3*) resembles the case of a planar surface, where $h \to \infty$ when $p/p_s \to 1$(curve *1*), in the smaller capillaries the isotherm breaks off at $p/p_s = 0.95$ (curve *2*) and $p/p_s = 0.45$ (curve *1*). The break-off of the isotherms corresponds to loss of the film of uniform thickness stability in accordance with Eq.s (13) and (33).

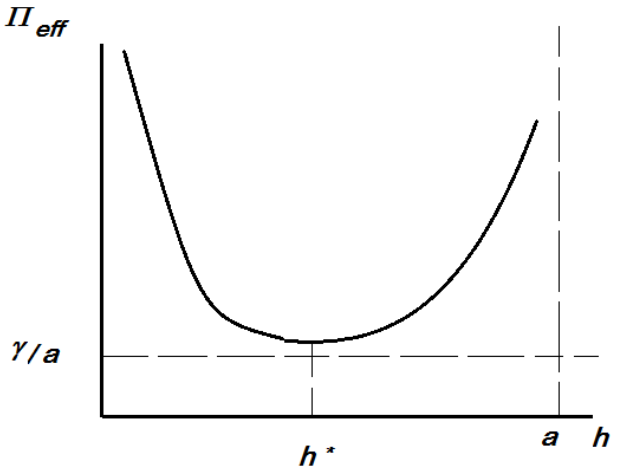

Fig. 5. Effective disjoining/conjoining pressure isotherm on the inner surface of a capillary of radius a in the case of complete wetting. Films of a uniform thickness are stable only if their thickness is less than h^*.For $h \geq h^*$, the film on the inner capillary surface loses stability, and the liquid changes over into a more stable state, forming a capillary condensate.

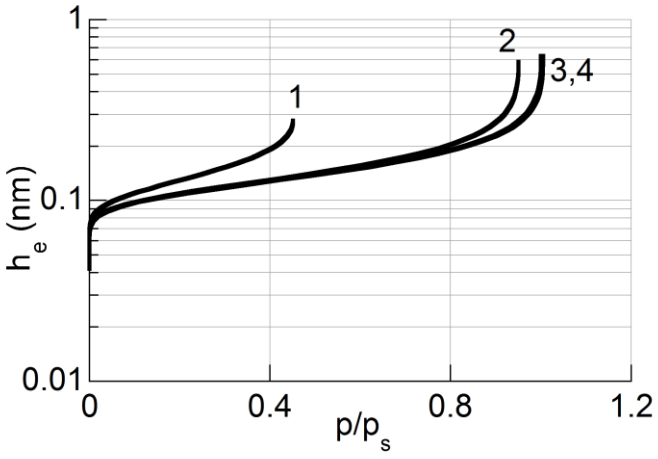

Fig. 6. Adsorption isotherms, $h(p/p_s)$, for films of water in quartz capillaries with radius a = 1 nm (curve *1*), 10 nm (curve *2*), 100 nm (curve *3*), and ∞ (curve *4*). Only those parts of the curves corresponding to stable films are shown.

6.2 Partial Wetting Case

When the contact angle is different from zero, a more complex shape of the disjoining/conjoining pressure isotherm has to be used in Eq. (28). Following the technique developed in [29] , we take into account the molecular, electrostatic and structural components of surface forces. The equation for disjoining pressure isotherm in SI units becomes:

$$\Pi(h) = \Pi_m(h) + \Pi_{el}(h) + \Pi_{st}(h) = \frac{A}{6\pi h^3} - \frac{\varepsilon\varepsilon_0\left(\varphi_1 - \varphi_2\right)^2}{2h^2} + K\exp(-h/\lambda) \qquad (37)$$

where subscripts *m*, *el* and *st* stand for 'molecular', 'electrostatic' and 'structural', respectively; A is the Hamaker constant; ε is the relative dielectric permittivity of liquid; ε_0 is electric constant; ϕ_1 and ϕ_2 are the electric potentials of the solid-liquid and liquid-air interfaces, respectively. 'The parameter K is positive in the case of forces of hydrophilic structural repulsion, and is negative in the case of forces of hydrophobic attraction.'[29] The decay length of structural forces, λ, is close in order of magnitude to the bulk correlation length, that is $\lambda \approx 1$ nm for water [29]. This equation can be used for small values of κh, where κ is the inverse Debye length, and when the surface potentials ϕ_1 and ϕ_2 are not dependent on film thickness [29].

According to this model, ignoring structural forces and accounting only for molecular and electrostatic ones gives contact angles not exceeding 60°. Therefore, it is necessary to use all three above-mentioned components of the disjoining/conjoining pressure to obtain higher contact angle values. In the case of water inside a carbon nanotube, contact angles comparable to those of water on graphite, in the 80-86° range, have been observed both experimentally and via molecular dynamics simulations [4]. As the water/graphite interface is not charged, and the water/air interface is charged, we have chosen the difference of surface potentials, $\Delta\phi = \phi_1 - \phi_2$, to be non-zero. The following parameters are used to obtain a contact angle of 80°: $A = 7\cdot10^{-21}$ J, $\varepsilon = 80$, $\Delta\phi = 0.05$ V, $K = -7.2\cdot10^7$ N/m^2, $\lambda = 1$ nm. The equilibrium thickness of the wetting film on a flat graphite surface in this case appeared to be 0.16 nm, which is less than the thickness of one monolayer. Physically it can be considered as a sparse monolayer. The shape of the disjoining/conjoining isotherm is shown in Fig. 7.

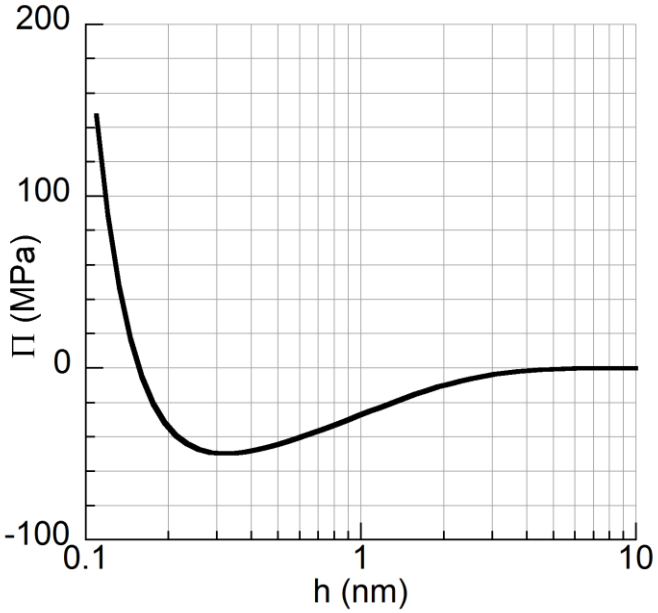

Fig. 7. Disjoining/conjoining pressure isotherm for water on flat graphite based on the Eq. (37) using parameters: $A = 7\cdot10^{-21}$ J, $\varepsilon = 80$, $\Delta\phi = \phi_1 - \phi_2 = 0.05$ V, $K = -7.2\cdot10^{7}$ N/m^2, $\lambda = 1$ nm.

Using the above disjoining/conjoining pressure isotherm we calculated the dependence of the equilibrium thickness, h_e, of the wetting film inside a graphitic nanotube of radius a as a function of the dimensionless vapour pressure p/p_s, where p_s is the saturated vapour pressure above the flat liquid-air interface according to the following equation $\frac{a}{a-h}\left(\Pi(h)+\frac{\gamma}{a}\right)=\frac{RT}{v_m}\ln\frac{p_s}{p}$, where the isotherm of the disjoining/conjoining pressure, Eq. (37) is used. This dependence is presented in Fig. 8.

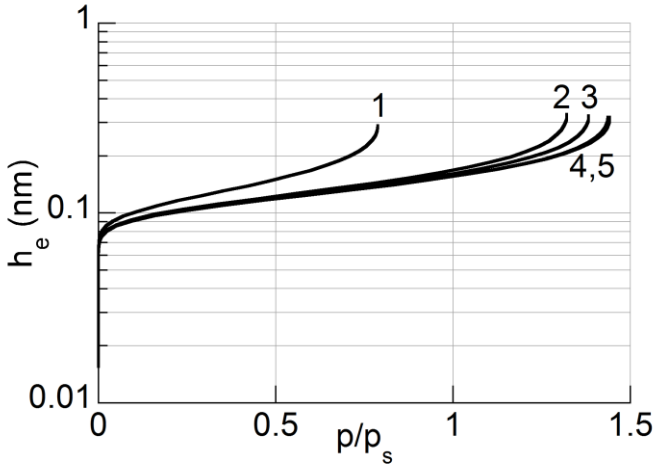

Fig. 8. Equilibrium thickness h_e of the wetting film on the inside wall of a graphitic nanotube as a function of vapour pressure, based on the disjoining pressure isotherm in Figure 7. The radius of the graphitic tube a is 1 nm (curve *1*), 5 nm (curve *2*), 10 nm (curve *3*), 100 nm (curve *4*), and ∞ (curve *5*). Only those parts of the curves corresponding to stable films are shown.

The condition of film stability is used for the determination of a stable range:

$$\frac{\partial \Pi_{eff}\left(h_e,a\right)}{\partial h_e}<0, \quad \text{where} \quad \Pi_{eff}\left(h_e,a\right)=\frac{a}{a-h_e}\left(\Pi(h_e)+\frac{\gamma}{a}\right)$$

Each curve in Fig. 8 ends with a point corresponding to the critical values of the film thickness, h_e^*, and vapour pressure p^*/p_s. When the vapour pressure (and accordingly the film thickness) exceeds the critical value, the wetting film becomes unstable and fills up the capillary. The dependences of the critical values h_e^* and p^*/p_s on a capillary radius, a, for the disjoining/conjoining pressure isotherm of a water/graphite system (Fig. 7) are shown in Fig. 9a and 9b.

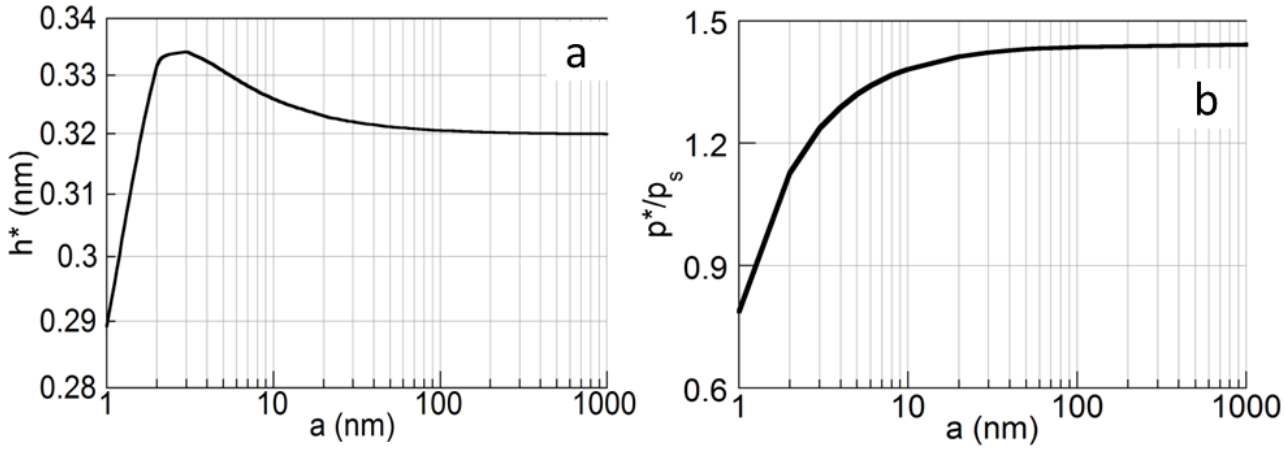

Fig. 9. a) Critical film thickness h^* and b) vapour pressure p^*/p_s in a capillary of radius a for a water/graphite system.

The shape of the curve in Fig. 9a is sensitive to the choice of parameters (K, λ, $\Delta\phi$) which are experimentally unknown: h^* can be a monotonically increasing or decreasing function of the capillary radius a, or have a maximum as in Fig. 9a. From Fig. 9b one can see that, for the above considered shape of the disjoining/conjoining pressure isotherm (Figure 7), in almost entire range of considered capillary radii a, the wetting film loses its stability and fills up the capillary at strong oversaturation of the vapour.

6.3 Limit of Validity of Continuum Model

In Figure 8, the condition $h<<a$ is fulfilled in the entire region of physically realizable film thicknesses, $h \le h^*$, for curves *2* to *5*. That is, capillary condensation starts much earlier than when the capillary is filled with liquid. Even though the thickness of adsorbed films with equal values of

p/p_s is bigger in a capillary with a smaller capillary radius, the region of their existence is curtailed quite substantially. When $h > h^*$, the films lose stability and the capillary is filled with condensate.

As discussed in the introduction, the validity of the continuum model on which this work is based has been called into question for liquids inside hydrophobic carbon nanotubes (and more in general in nanoscale channels) with radius as small as 1-2 nm. As such, one has to question whether the condition $h \ll a$ is satisfied for the smallest capillaries, for example $a = 1\,\text{nm}$, in Fig. 8. As can be seen in Fig.s 9a and 9b the approximation $h \ll a$ can no longer be considered valid below a radius size $a \sim 1-2\ \text{nm}$. This result confirms molecular dynamics and experimental observations showing a breakdown of the continuum model below ~ 2nm [20, 21].

7. Line Tension

In the above calculations of macroscopic contact angles and/or stability of layers of a uniform thickness, the line tension term [30] is absent. This is due to the choice of considering a 'real' drop profile which includes a transition zone between the droplet and the liquid film absorbed on the solid surface (Fig. 10a). This complex profile results from the action of capillary and surfaces forces (disjoining/conjoining pressure), as discussed in Section 1. On the other hand, if one replaces the real profile with an idealised one, where the spherical cap is extended down to a sharp intersection with the liquid film of a uniform thickness (Fig. 10b), then along a new apparent three phase contact line a line tension should be introduced. It is finally noted that the line tension can be calculated from the more general model presented here according to a procedure described in [2].

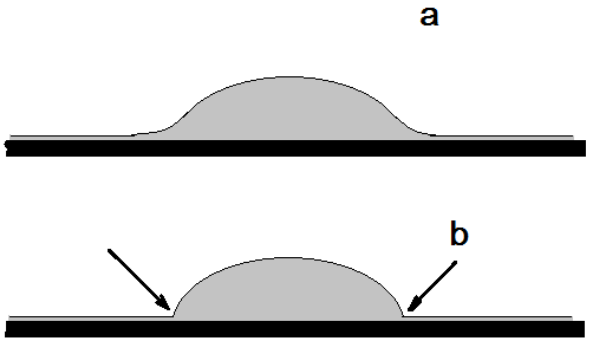

Fig. 10. a) Real liquid profile calculated using the disjoining pressure isotherm, Eq. (6); b) Idealized liquid profile, where a spherical cap is extended down to a sharp intersection with a thin liquid film a the apparent three phase contact line (arrows).

8. Conclusions

The properties of films on curved surfaces that have been examined, i.e., film stability and thickness, should be taken into account in investigating adsorption processes in fine-porous solids, wetting of nanostructured surfaces, and flow of liquids through nanotubes and nanochannels.

An effective disjoining/conjoining pressure isotherm has been deduced for liquid films of uniform thickness on an inner or an outer cylindrical surface, with the effective disjoining/conjoining pressure being a function of the surface curvature. From the latter, the equilibrium contact angles of drops on an outer or inner surface of a cylindrical capillary have been calculated, showing that the expressions for equilibrium contact angles vary from the case of a drop on a flat surface, in view of the difference in thickness of the film of uniform thickness with which the bulk liquid (drops or menisci) is at equilibrium.

Calculations for water in hydrophilic quartz nanocapillaries and hydrophobic carbon nanotubes have confirmed MD and experimental results showing a size threshold below which the continuum model no longer applies due to the effects of nanoscale confinement.

ACKNOWLEDGMENT: DM acknowledges the support of UK Royal Academy of Engineering through a Research Fellowship. VS and SS research was supported by MULTIFLOW project, EU and PASTA project, European Space Agency. The authors thank the Reviewers for the useful comments on line tension.

REFERENCES

[1] B.V. Derjaguin, et al., Surface Forces. Consultants Bureau/Plenum Publishing Co, 1987.
[2] V.M. Starov, et al., Wetting and Spreading Dynamics. CRC Press, BOca Raton, FLorida, 2007.
[3] M. Whitby, N. Quirke, Nat. Nano. 2 (2007) 87.
[4] D. Mattia, Y. Gogotsi, Microfluid. Nanofluid. 5 (2008) 289.
[5] J.N. Coleman, et al., Advanced Materials 18 (2006) 689.
[6] P.J.F. Harris, Int. Mater. Rev. 49 (2004) 31.
[7] M.Q. Tran, et al., Nano Lett. 8 (2008) 2744.
[8] T. Arai, et al., J. Polym. Sci. Pt. B-Polym. Phys. 43 (2005) 2568.
[9] S.M. Hong, et al., Mol. Cryst. Liquid Cryst. 464 (2007) 777.
[10] S. Bekou, D. Mattia, COCIS 16 (2011) 259.
[11] H. Sato, M. Sano, Colloids and Surfaces A: Physicochemical and Engineering Aspects 322 (2008) 103.
[12] D. Mattia, F. Calabrò, Microfluid. Nanofluid. (2012) 1.
[13] S. Chibbaro, et al., Journal of Statistical Mechanics-Theory and Experiment (2009).
[14] M.P. Rossi, et al., Nano Lett. 4 (2004) 989.
[15] D. Mattia, et al., J. Phys. Chem. B 110 (2006) 9850
[16] T. Myers, Microfluid. Nanofluid. 10 (2010) 1141.
[17] J.A. Thomas, et al., International Journal of Thermal Sciences 49 (2010) 281.
[18] J.W. van Honschoten, et al., Chem. Soc. Rev. 39 (2010) 1096.
[19] A. Nikolov, et al., Langmuir 26 (2010) 7665.
[20] J.A. Thomas, A.J.H. McGaughey, Phys. Rev. Lett. 102 (2009) 184502.
[21] D. Mattia, et al., in: (Ed.)^(Eds.)5th IASME/WSEAS International Conference on Fluid Mechanics and Aerodynamics, Athens, Greece, 2007, p 297.
[22] N. Naguib, et al., Nano Lett. 4 (2004) 2237.
[23] S. Nuriel, et al., Chem. Phys. Lett. 404 (2005) 263.
[24] M.Q. Tran, et al., Nano Letters 8 (2008) 2744.

[25] M.P. Rossi, et al., Langmuir 25 (2009) 2804.
[26] J. Israelachvili, Intermolecular & Surface Forces. Second ed., Academic Press, San Diego, CA, 1991.
[27] N.V. Churaev, Colloid Journal 36 (1974) 318.
[28] B.V. Derjaguin, et al., Colloid Journal 37 (1975) 219.
[29] N.V. Churaev, V.D. Sobolev, Adv. Colloid Interface Sci. 61 (1995) 1.
[30] J.S. Rowlinson, B. Widom, Molecular Theory of Capillarity. Clarendon Press, Oxford, UK, 1982.